ChemCatChem

Supporting Information

Engineering CYP153A$_{M.aq}$ to Oxyfunctionalize its Inhibitor Dodecylamine Using a LC/MS Based Rapid Flow Analysis Screening

Lea R. Rapp, Sérgio M. Marques, Bernd Nebel, Jiri Damborsky, and Bernhard Hauer*

EXPERIMENTAL STUDIES

Unless otherwise stated, all reagents were purchased in analytical grade from Sigma-Aldrich (Steinheim, Germany), Carl Roth (Karlsruhe, Germany), Merck and VWR (Darmstadt, Germany) and Alfa Aesar (Karlsruhe, Germany). Oligonucleotides were synthesized by Metabion International AG (Martinsried, Germany). DNA sequencing was performed by GATC Biotech (Konstanz, Germany).

Strains and plasmid construction. *Escherichia coli* strain XL1-Blue was obtained from Stratagene (Agilent, St. Clara, USA) and BW25113ΔfadD from the National Institute of Genetics (Mishima, Japan). The plasmid encoding the artificial fusion construct CYP153A$_{M.aq}$-PFOR L2 within the vector pBAD33 were described previously.[1,2] Saturation with the "22c-trick" was performed on pBAD33_ CYP153A$_{M.aq}$-PFOR L2 as described elsewhere using respective oligonucleotides (**Table S1**).[3] The DNA products were transformed into competent XL1-Blue cells for the reproduction of the plasmid DNA and extracted with the Zyppy Plasmid Miniprep Kit from ZYMO Research (Freiburg, Germany) and the correct distribution of the bases was confirmed by DNA sequencing.

Table S1: Oligonucleotide sequences for saturation mutagenesis.

Mutation		**Sequence** (5'- to 3'-direction)
Q129X	fwd 1	CTGTTTTCCGCCGAGCCGndtATCATTCTCGGTGACCCTCCG
	fwd 2	CTGTTTTCCGCCGAGCCGvhgATCATTCTCGGTGACCCTCCG
	fwd 3	CTGTTTTCCGCCGAGCCGtggATCATTCTCGGTGACCCTCCG
	rev	CGGCTCGGCGGAAAACAGGTCGTGACTCTTATCCACGAACAGG
V141X	fwd 1	CTCCGGAGGGGCTGTCGndtGAAATGTTCATAGCGATGGATCCG
	fwd 2	CTCCGGAGGGGCTGTCGvhgGAAATGTTCATAGCGATGGATCCG
	fwd 3	CTCCGGAGGGGCTGTCGtggGAAATGTTCATAGCGATGGATCCG
	rev	CGACAGCCCCTCCGGAGGGTCACCGAGAATGATTTGCGGC
M228X	fwd 1	GCTGGTTGAGTGGTCGGACAGAndtGCAGGTGCAGCATCG
	fwd 2	GCTGGTTGAGTGGTCGGACAGAvhgGCAGGTGCAGCATCG
	fwd 3	GCTGGTTGAGTGGTCGGACAGAtggGCAGGTGCAGCATCG
	rev	TCTGTCCGACCACTCAACCAGCTTGTGGCGTTCCTCGTAAGGAAAATC

Cultivation, expression and biotransformation in 96-deepwell plates. The plasmid mixture obtained with the "22c-trick" was transformed into competent BW25113ΔfadD cells and single colonies were picked using sterile toothpicks to inoculate a 96-deepwell plate (2 mL Riplate®, Carl Roth, Karlsruhe, Germany) with 500 µL LB-Lennox containing 34 µg/mL chloramphenicol (LB-Cmp) per well. Plates were sealed with Breath-EASIER sealing membranes (Diversified Biotech, Dedham, Massachusetts, USA) and incubated at 37 °C and 250 rpm overnight. 50 µL of this preculture were used to inoculate 650 µL Terrific Broth containing 34 µg/mL chloramphenicol (TB-Cmp) and incubated for 4 h at 37 °C and 250 rpm. Gene expression was induced with 0.02% arabinose, 0.5 mM 5-aminolevulinic acid (5-ALA) and 0.1 mM $FeCl_3$ and incubated for 20 h at 25 °C and 250 rpm. To prepare resting cells, cell pellets were resuspended after harvesting in 500 µL working buffer (0.1 M potassium phosphate buffer, pH 7.4) supplemented with 1% glycerol and 0.5 mM glucose. For the biotransformation 10 µL of a 50 mM dodecylamine solution in pure ethanol (EtOH) were added to the resting cells and incubated for 4 h at 30 °C and 250 rpm. The reaction was stopped by adding 90 µL of 5 M NaOH and subsequent incubation for 15 min at 250 rpm. For the extraction, 500 µL acetonitrile was mixed by pipetting the mixture up and down and phase separation was achieved by centrifugation for 10 min at 4000 x g.

Mass Spectometry-based Rapid-flow Analysis of Product Peaks (RAPP). The MS-based Rapid-flow Analysis of Product Peaks (RAPP) was established to receive a fast and reliable quantitative detection of the hydroxylation of dodecylamine. Because only the total molecular masses were hunted, this analysis served as an extremely rapid and precise (no false positives) prescreening without exact quantification of the analytes or position of the hydroxylation. Biotransformations with normalized P450 concentration were subsequently conducted to compare the variants and quantify the ω-hydroxylated product.

For the direct and Rapid Flow Analysis, an LC-ESI/MS system consisting of a binary pump and an ESI single-quadrupole MS detector (Agilent 6130) was used. FIA series were enabled in the method to capture the RAPP in a single chromatogram and the system was operated at 30 °C without any chromatographic column to separate the analytes. 0.5 µL of each sample was injected every 36 sec in a constant flow rate of 0.45 mL/min of the mobile phase (25% ddH_2O with 0.1% formic acid and 75% acetonitrile) and the pressure limit was set to 80 bar. Needle and valve cleaning was enabled for 5 sec before each sample to avoid cross-contamination of the analytes. To ensure direct sampling from the organic phase in the 96-deepwell plates, the draw position of the needle was adjusted to 16 mm. The detection was performed using an ESI/MS detector. Drying gas temperature 350°C, flow 10 L min-1; nebulizer pressure 30 psig; capillary voltage + 4000 V, single ion mode (SIM) dodecylamine: *m*/*z* 186 and hydroxylated product: *m*/*z* 202.

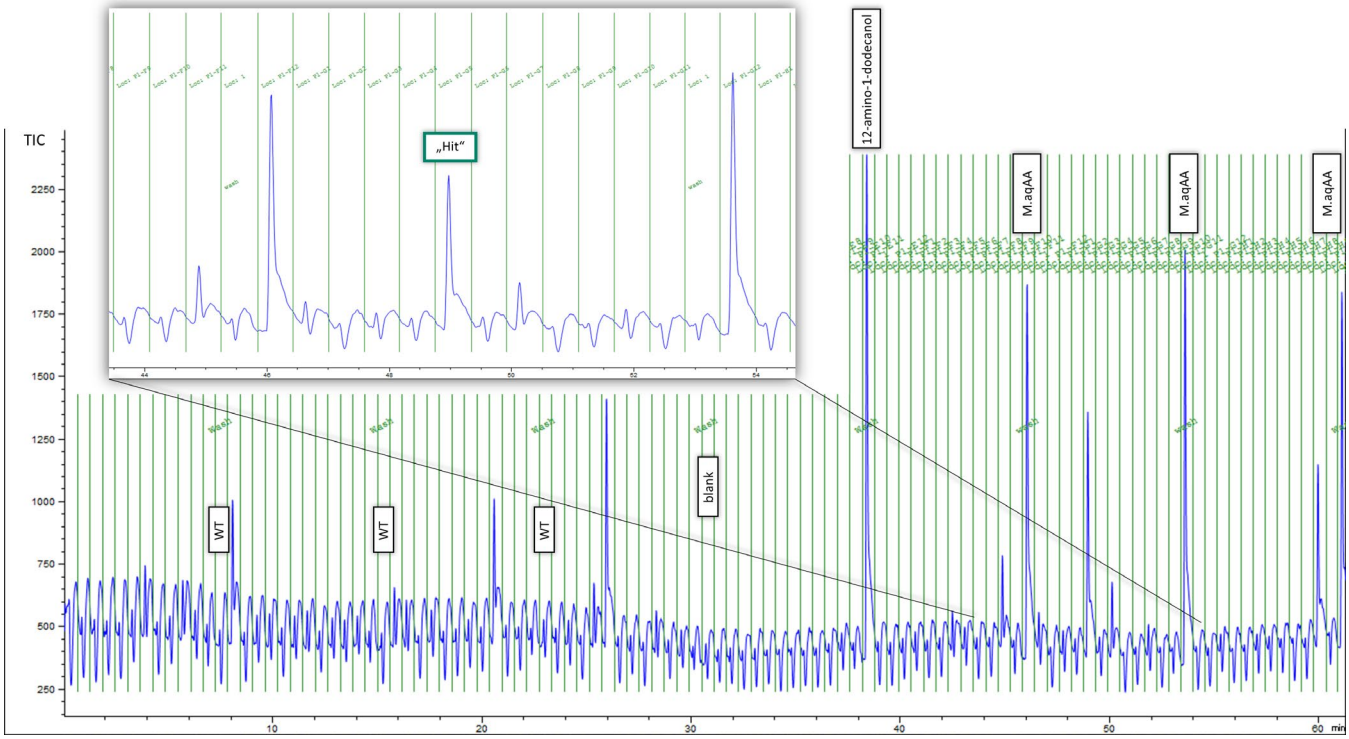

Figure S1: Chromatogram of a single RAPP run with 96 injected samples and 8 washing steps (64 min). The chromatogram shows the results for the saturation of the amino acid Q129 with the wild type as parent. Each sample is separated by a green line. A control was run after each wash: Wild type negative control (WT); blank (no cells); 12-amino-1-dodecanol (product standard); positive control initial variant (M.aqAA). The Total Ion Count (TIC) of the hydroxylated dodecylamine product (*m*/*z* 202) is presented. The zoomed section shows an example of a “Hit” selected for sequencing and validation.

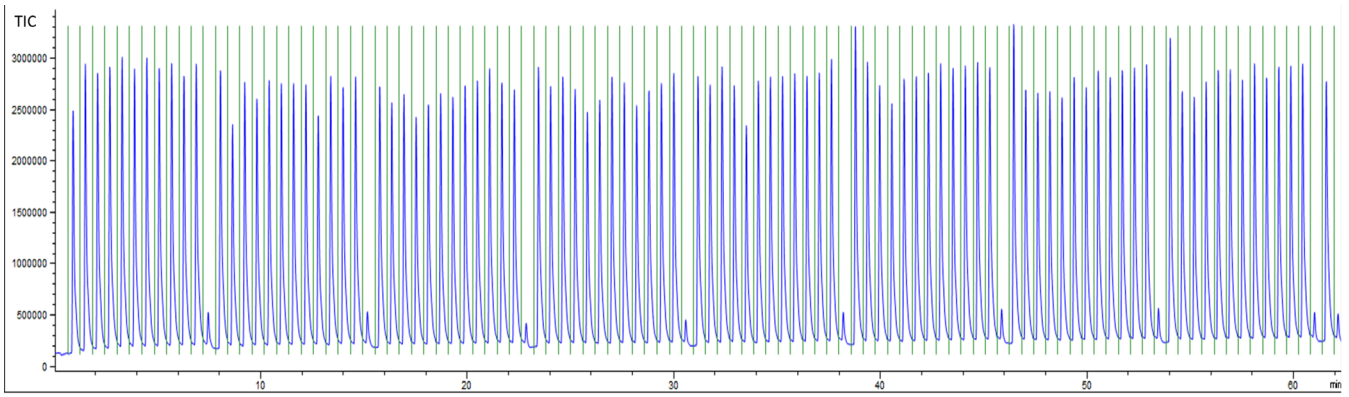

Figure S2: Chromatogram of a single RAPP run with 96 injected samples and 8 washing steps (64 min). Each sample is separated by a green line. A blank control was measured after every 11 samples . The Total Ion Count (TIC) of the dodecylamine substrate (*m/z* 186) is presented.

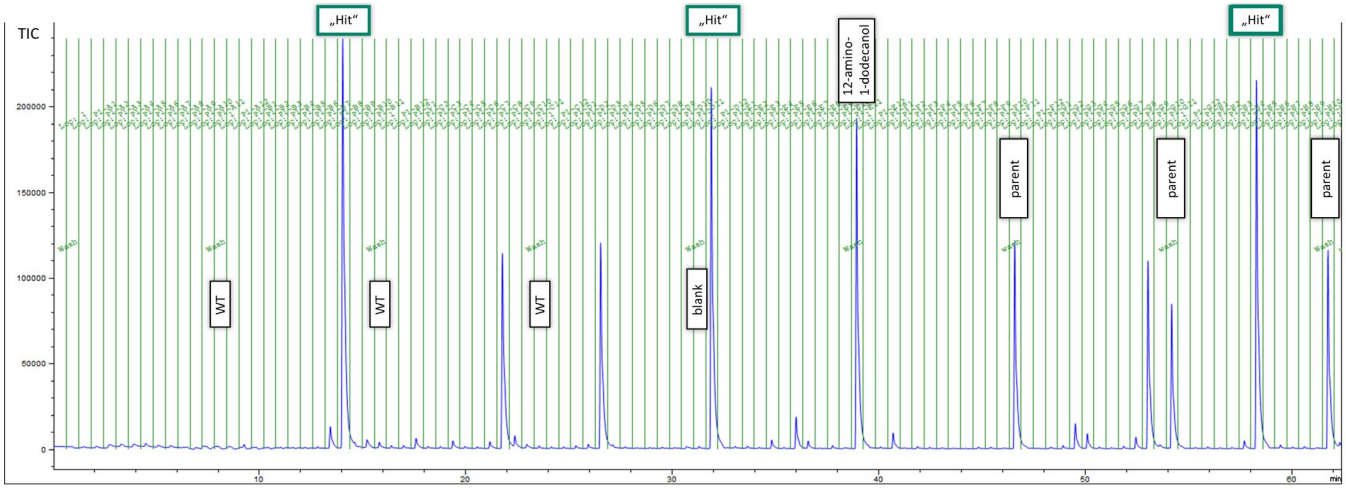

Figure S3: Chromatogram of a single RAPP run with 96 injected samples and 8 washing steps (64 min). The chromatogram shows the results for the saturation of the amino acid V141 with M.aqEE as parent. Each sample is separated by a green line. A control was run after each wash: Wild type negative control (WT); blank (no cells); 12-amino-1-dodecanol (product standard); parent control (M.aqEE). The Total Ion Count (TIC) of the hydroxylated dodecylamine product (*m/z* 202) is presented.

Protein expression and determination of concentration for the verification of hits. Plasmids harbouring genes of the wild type or variants of CYP153A$_{M.aq}$ were always freshly transformed and single colonies were used for overnight cultures in LB-Cmp. 0.25 mL of the preculture was used to inoculate 50 mL TB-Cmp. Overexpression was induced with 0.02% arabinose when the optical density at 600 nm (OD_{600}) of the cultures reached 0.8 – 1 and supplemented with 0.5 mM 5-ALA and 0.1 mM $FeCl_3$. The cells were harvested after 16 h incubation at 25 °C and 180 rpm by centrifugation at 4 °C and subsequent resuspension in working buffer. The cells were lysed on ice via sonication with a duty cycle of 30% for 5 min and insoluble debris was removed by centrifugation. The CO difference spectral assay[4] was modified for P450 concentration determination with CO gas saturated working buffer using $\varepsilon_{450-490} = 91\ mM^{-1}\ cm^{-1}$. Respective samples without CO treatment were subtracted as corresponding blank samples. For the wild type, single and double variants, dodecanoic acid was used as the reducing agent to determine the concentration of the active fusion construct. Only for the variant M.aqESE $Na_2S_2O_4$ was used as reducing agent since this variant did not accept dodecanoic acid.

The heme domains without fusion of the reductase domain and the reductase partners CamA and CamB that were used for the kinetic analyses were cultivated, expressed and purified as described by Rapp *et al*.[5] This system was used to ensure an excess of reductase partners so as not to distort kinetics.

Enzymatic hydroxylation reactions for the verification of hits. Biotransformations to verify the hits found in the prescreening were performed *in vitro* in a final volume of 0.17 mL in 0.1 M potassium phosphate buffer (pH 7.4) containing 1 µM P450, 1 mM NADPH, 1 mM $MgCl_2$, 5 mM glucose-6-phosphate and 2 U glucose-6-phosphate dehydrogenase from *Leuconostoc mesenteroides* for cofactor regeneration. Reactions were initiated by the addition of 1 mM dodecylamine (50 mM stock in EtOH) and incubated at 30 °C and 550 rpm for 4 h in a thermo shaker (Thermomixer comfort, Eppendorf AG, Hamburg, Germany). The reactions were stopped by the addition of 30 µL 5 M NaOH and frozen until extraction for analysis.

Kinetic analysis. In order to determine the IC_{50} of dodecylamine, kinetics for the model substrate, dodecanoic acid, had to be realized. The activities of the wild type and variant M.aqAA were assessed *in vitro* by performing described biotransformations using 0.1 to 0.3 µM P450 heme domain with a 1:5:10 ratio of P450, CamA and CamB,

respectively. Concentrations of the substrate dodecanoic acid (in DMSO) were varied between 0.01 – 1 mM (for solubility reasons) and the reactions were incubated as described above but stopped after 10 – 20 min within the constant rate range (steady-state). The Michaelis-Menten equation ($v = v_{max}*[S]/(K_m+[S])$) and the Excel Solver plugin were used to fit the kinetic parameters. For the calculation of the specific activity, the mass of CYP153A$_{M.aq}$ was used as 54 kDa. For the substrate excess inhibition, the dissoziation constant K_i has been set equal to K_m and the equation was modified to $v = v_{max}/(1+(K_m/[S])+([S]/K_m))$.

For the effector kinetics, 0.12 mM of dodecanoic acid was used because the greatest influence of the effector was expected at this concetration (K_m). The inhibitor dodecylamine was varied between 0.078 µM – 1 mM. Due to the binding of the dodecylamine in the active site, we expected the fit being similar to competitive inhibition and used the equation $v = (v_{max}*[S_0])/([S_0]+K_m*(1+[I]/K_i))$ and the Excel Solver plugin to fit the kinetic parameters assuming that K_m remains constant. IC_{50} results as the concentration of the inhibitor at which the activity was reduced to 50% of the activity without inhibition.

To determine kinetic values with dodecylamine as inhibitor at the IC_{50} and dodecanoic acid as substrate, dodecylamine was used at the respective IC_{50} of 0.9 µM for M.aqWT and 2.5 µM for M.aqAA and the concentration for dodecanoic acid was varied between 0.01 – 1 mM (for solubility reasons) and incubated as described above.

GC-FID analytics. The dodecanoic acid and the formed product was analysed as described previously.[5] Samples with biotransformations for the verification of hits containing dodecylamine and the corresponding hydroxylated products were extracted with 0.2 mL methyl *tert*-butyl ether (MTBE) containing 5% acetic anhydride until derivatization and addition of 0.1 mM undecylamine as the internal standard. The mixture was vortexed 2 min for complete derivatization and the organic phase was transferred into a GC vial. Dodecylamine and 12-amino-1-dodecanol were analyzed by GC-FID using a Shimadzu GC-2010 GC system with FID detector, equipped with a CP-Sil 8 CB column (30 m x 0.25 mm x 0.25 µm, Agilent. Santa Clara, USA) and quantified with calibration curves between 0.01 – 1 mM from the corresponding standards (≥ 98% purity). Helium was used as the carrier gas at a linear velocity of 40 cm/sec. The injector and detector temperatures were set to 280 °C and 325 °C, respectively. 1 µL of each sample was injected and measured with a split of 10. The method program was as follows: Start at 200 °C and increase to 250 °C at 20 °C per min and then rise to 310 °C at 35 °C per min, keeping the temperature constant for 1 min.

Spin-state analysis. To determine the spin-state shifts upon binding of the ligand, the spin-shift was monitored at 30 °C, carried out and calculated as described by Klenk *et al*.[6] with the exception of dodecylamine being dissolved in EtOH. Concentrations were varied between 5 and 1250 µM dodecylamine and 1 µM P450 lysate was used.

Computational studies

***In silico* mutagenesis, ligand and receptor preparation.** The model of M.aqAA (two amino acid substitutions: V141A, M228A), M.aqEE (two amino acid substitutions: Q129E, M228E) and M.aqESE (three amino acid substitutions: Q129E, V141S, M228E) were constructed by *in silico* mutagenesis as described previously.[5] The structures of the dodecylamine and 12-amino-1-dodecanol were constructed and minimized using Avogadro[7]. The subsequent ligand and receptor preparation was described previously.[5]

Molecular docking in the active site. Was carried out as described previously.[5] The input files of the receptors and respective ligands in pdb format were converted into the AutoDock Vina-compatible pdbqt format using MGLTools.[8] The partial charge of the iron atom in the receptors was subsequently set to 0.25, as calculated elsewhere.[9] For the molecular docking performed by AutoDock Vina[10], the active site of CYP153A$_{M.aq}$ wild type and variants was selected as the region of interest. This region was represented by a box of 15 × 16.88 × 15 Å located above the heme and defined to include the tunnels 2c and 2e. For the calculations, exhaustiveness of 50 was used.

System preparation, equilibration, MD simulation and post-processing analysis.

The system was prepared, equilibrated, MD simulations were computed and post-simulation treatment and analysis of the MDs were performed as described previously.[5] The proteins were hydrated with the water molecules from the crystal structure of the wild type CYP153A$_{M.aq}$ (PDB entry 5FYG) and any water overlapping with the protein atoms was removed. The tLEaP program of AmberTools 14[11] was used to prepare the topology and trajectory input files for the dynamics simulation. For this purpose, the ff14SB force field[12] was specified and the parameters for the heme and heme-bound cysteine residues in the enzymes were added as obtained from the literature for the penta-coordinate ferric high-spin sextet state (IC6).[9] The Na^+ ions required to neutralize the system were added, as well as a truncated octagonal box of OPC3[13] water molecules with the edges 10 Å away from the original system.

The molecular dynamics (MD) simulations were carried out with PMEMD.CUDA[14,15] module of AMBER 14[11]. In total, five minimization steps and twelve steps of equilibration dynamics were performed prior to the production MD. The first four minimization steps, composed of 2,500 cycles of steepest descent followed by 7,500 cycles of the conjugate gradient, were performed as follows: (i) in the first one, all the atoms of the protein were restrained with 500 kcal/mol·Å^2 harmonic force constant; (ii) in the following ones, only the backbone atoms of the protein were restrained, with 500, 125, and 25 kcal/mol·Å^2 force constant. A fifth minimization step, composed of 5,000 cycles of steepest descent and 15,000 cycles of the conjugate gradient, was performed without any restraints. The subsequent MD simulations employed periodic boundary conditions, the particle mesh Ewald method for treatment of the long-range interactions beyond the 10 Å cutoff[16], the SHAKE algorithm[17] to constrain the bonds involving the hydrogen atoms, the Langevin thermostat with collision frequency 1.0 ps-1, and a time step of 2 fs. Equilibration dynamics were performed in twelve steps: (i) 20 ps of gradual heating from 0 to 300 K, under constant volume, restraining the protein and ligand atoms with 200 kcal/mol·Å^2 harmonic force constant; (ii) ten MDs of 400 ps each, at constant pressure (1 bar) and constant temperature (300 K), with gradually decreasing restraints on the backbone atoms of the protein and heavy atoms of the ligand with harmonic force constants of 150, 100, 75, 50, 25, 15, 10, 5, 1, and 0.5 kcal/mol·Å^2; (iii) 400 ps of unrestrained MD at the same conditions as the previous restrained MDs. The energy and coordinates were saved every 10 ps. The production MDs were run for 200 ns using the same settings employed in the last equilibration step, and they were performed in quintuplicate for the wild type enzyme and the M.aqESE variant (in a total simulation time of 1 μs), and in triplicate for the M.aqAA variant (in a total of 600 ns). To obtain more signigicant results, we simulated the more important systems (the wild type and M.aqESE) in a higher number of replicates. The trajectories were centered, stripped of all water molecules and ions, and aligned to the respective initial structures by minimizing the root-mean-square deviation (RMSD) of the backbone atoms using the cpptraj[18] module of AmberTools 14. The trajectories were visualized using PyMOL 2.0[19] and VMD 1.9.1[20].

Tunnel calculation. CAVER 3.02[21] was used as the standalone version to identify the protein tunnels in the MD simulations of the wild type CYP153A$_{M.aq}$ and the variant M.aqAA. The plugin for PyMOL was used to compute the tunnels in the crystal structure of the wild type and the homology models of the variants.

The tunnels were calculated as previously described with a probe radius of 0.9 Å, and a tunnel was considered being “open” if its bottleneck radius was equal to or greater than 1.4 Å.

Supplementary tables and figures

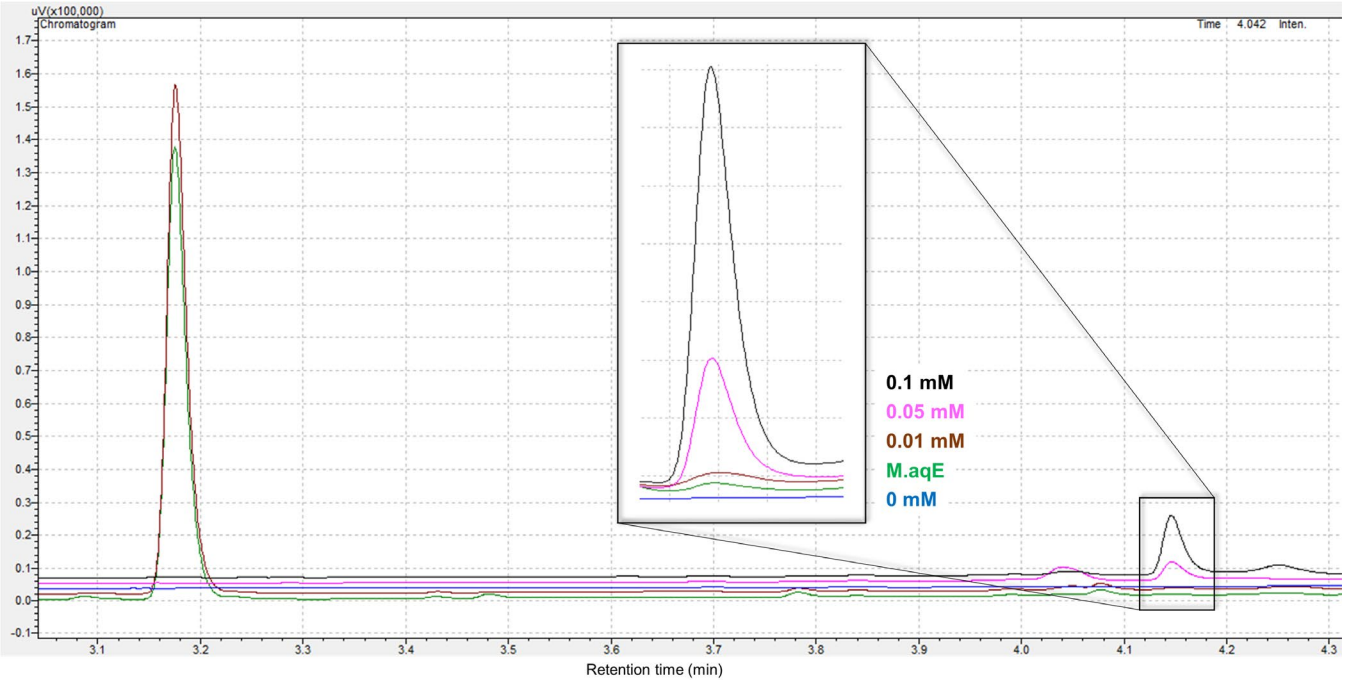

Figure S4: GC/FID Chromatogram of product standards (12-amino-1-dodecanol) and biotransformation of M.aqE. Peak at 4.15 min: 12-amino-1-dodecanol; 0.1 mM (black), 0.05 mM (pink), 0.01 mM (brown), M.aqE (green) and 0 mM (blue).

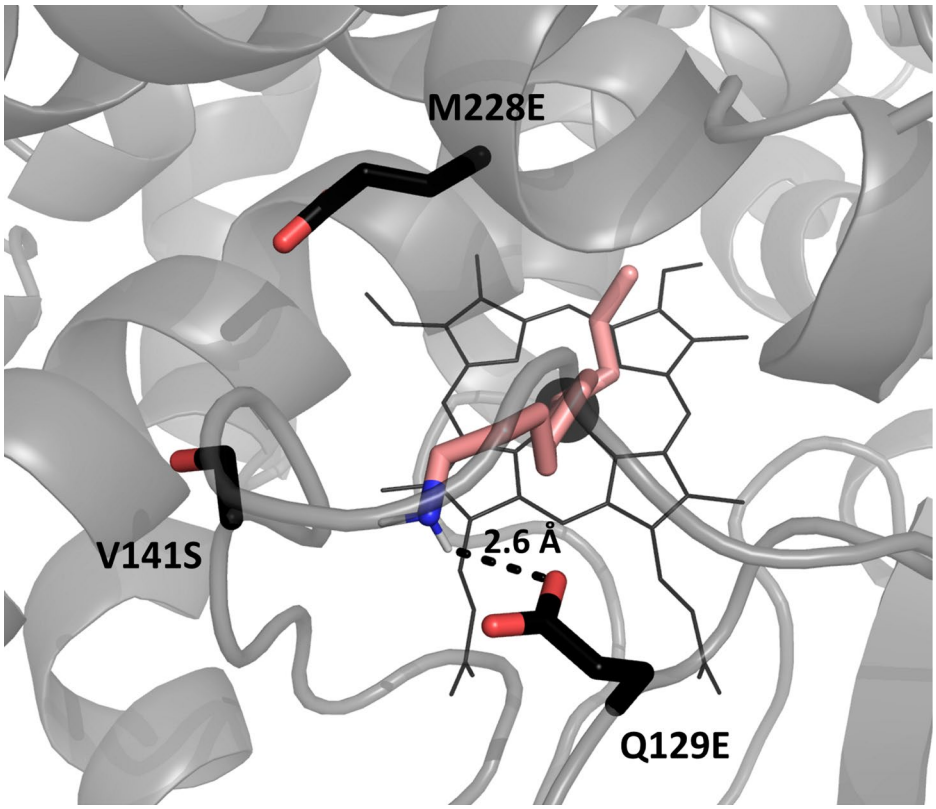

Figure S5: M.aqESE with docked dodecylamine (salmon). The N-H-O binding is indicated with a distance of 2.6 Å and a binding energy of -4.9 kcal/mol. The heme is represented as black lines and the iron as sphere.

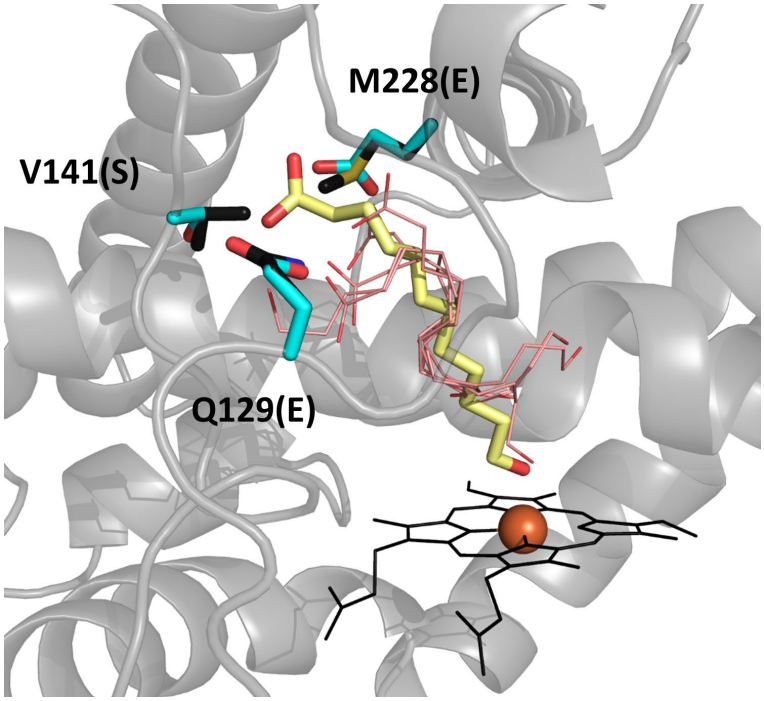

Figure S6: M.aqWT (black) with the co-crystallized ω-hydroxy-dodecanoic acid (yellow) and M.aqESE (cyan) with docked ω-hydroxy-dodecanoic acid (salmon). The five best docking modes are presented for M.aqESE to demonstrate the repulsion of the acid group by the introduces glutamates. The heme is represented as black lines and the iron as an orange sphere.

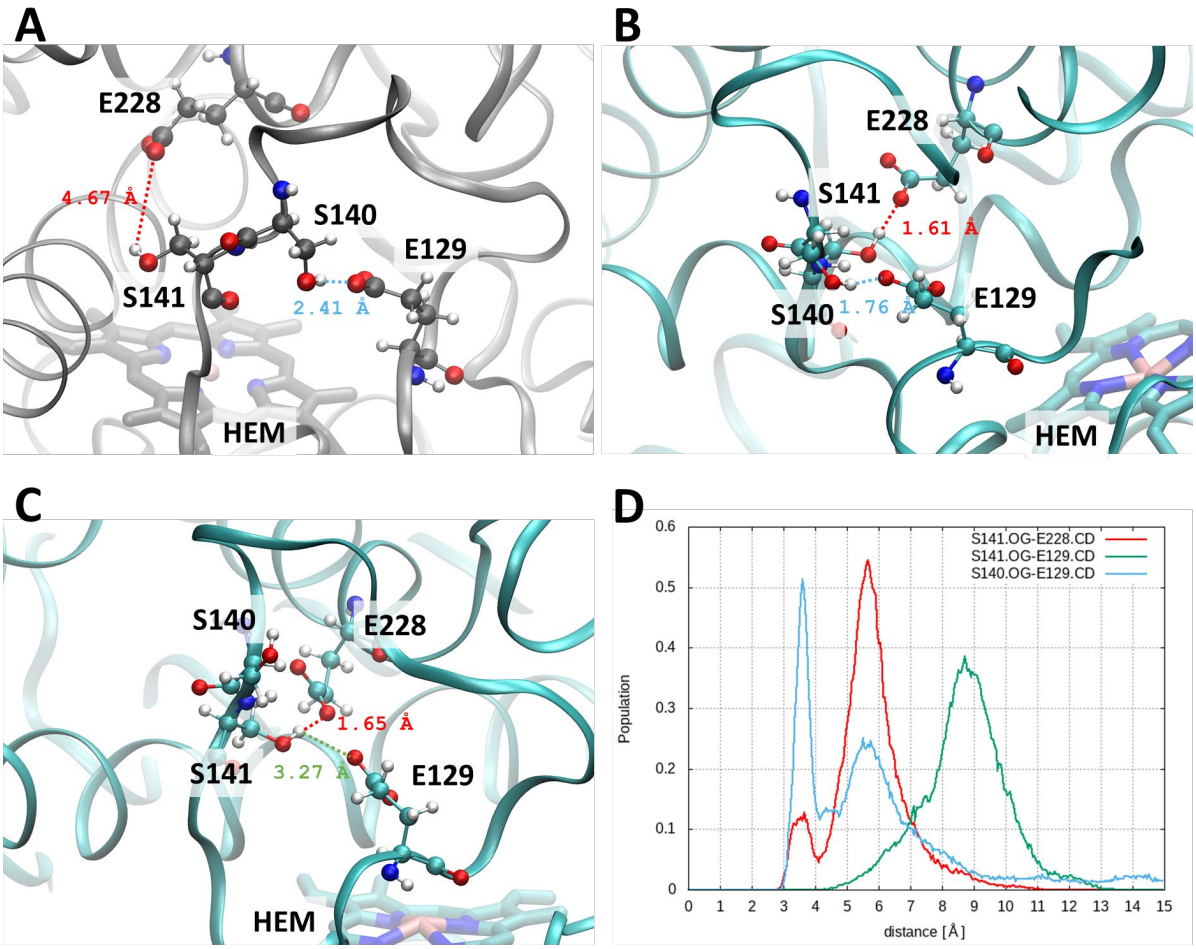

Figure S7. Position of the mutated residues (Q129E, V141S, and M228E) in the MaqESE variant and potential hydrogen-bonds formed during the respective MDs. A) The structure of MaqESE modelled *in silico*; B and C) two snapshots from the MD simulation where the mutated residues formed hydrogen bonds with one other and with S140; D) histogram distribution of the distances associated with the hydrogen bonds represented in the structures, computed for the entire set of MDs (distances calculated for the heavy atoms S140-Oγ, S141-Oγ, E129-Cδ, and E228-Cδ). The mutated residues are represented as CPK, the heme as licorice, the protein as ribbons, and the distances of potential hydrogen bonds as dotted lines; the distances in panel D are represented in the same colors as the respective hydrogen bonds displayed in the panels A-C.

Globally, we can observe that S141 forms a hydrogen bond with E228 in a significant number of snapshots (red curve, distance S141-Oγ-E228-Cδ ≤ 4 Å). S140 forms a hydrogen bond with E129 in the majority of the snapshots (blue curve, S140-Oγ-E129-Cδ ≤ 4 Å), stabilizing it in a position that may be advantageous for interacting favourably with the amine group of dodecylamine. A hydrogen bond between S141 and E129 was also observed, as represented in panel C, although only in a small number of snapshots (green curve, distance S140-Oγ-E129-Cδ ≤ 5 Å).

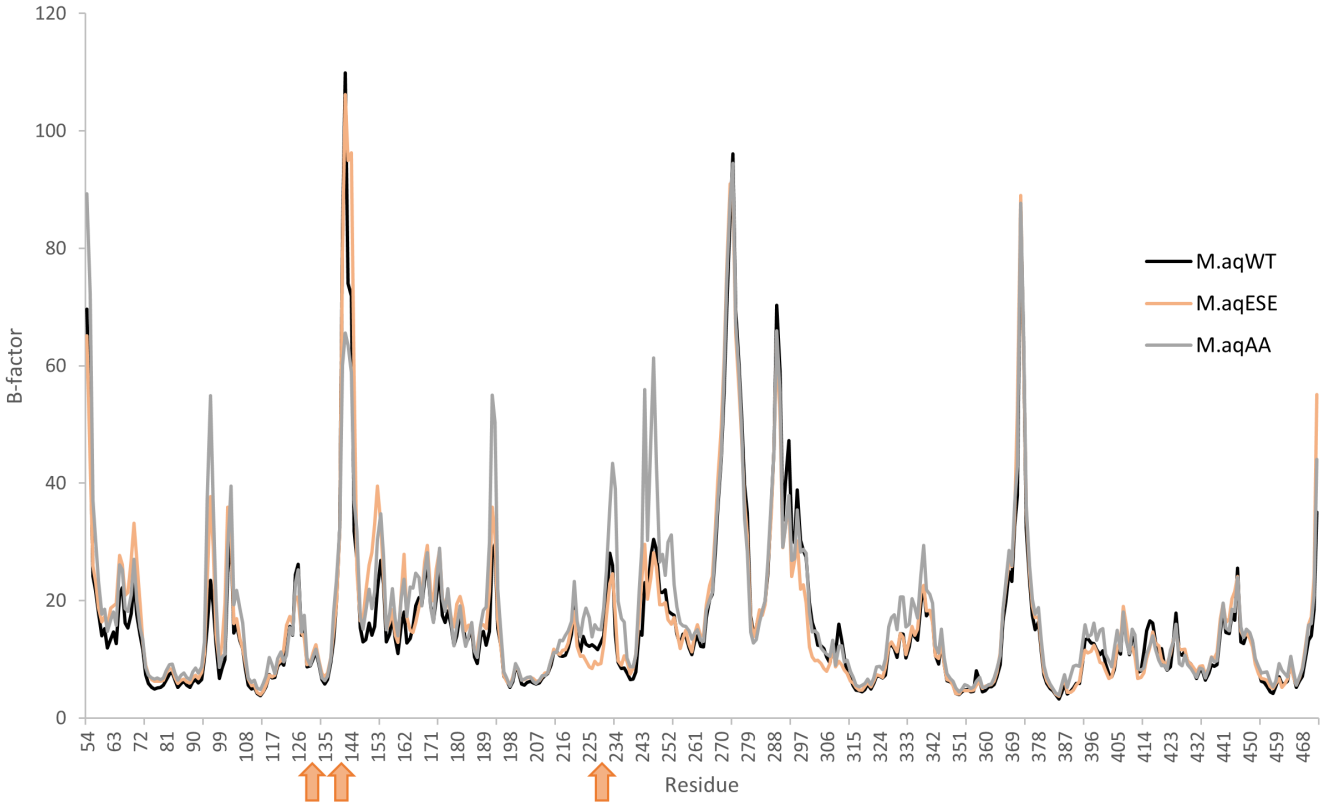

Figure S8: B-factors of the enzymes residues: The enzyme wild type M.aqWT (black), the variant M.aqAA (grey) and the variant M.aqESE (orange). B-factors were calculated as the average among the four individual MD simulations, respectively. The position of the mutations in M.aqESE are pointed out by the orange arrows.

Table S2: Product formations of the wild type and the engineered variants.

Variant	12-amino-1-dodecanol (µM)	ω-hydroxy dodecanoic acid (µM)
M.aqWT	n.d.	390.36 ± 23.59
M.aqAA	2.13 ± 0.27	180.27 ± 6.59
M.aqEE	4.22 ± 0.54	27.75 ± 3.12
M.aqESE	37.85 ± 3.21	6.74 ± 0.98

Conditions: 1 µM P450, 1 mM substrate, 2 % DMSO (dodecanoic acid) or EtOH (dodecylamine), 1 mM NADPH and cofactor regeneration, 100 mM potassium phosphate buffer, pH 7.4, 550 rpm, 30 °C, 1 h (dodecanoic acid) or 4 h (dodecylamine). n.d. not detectable

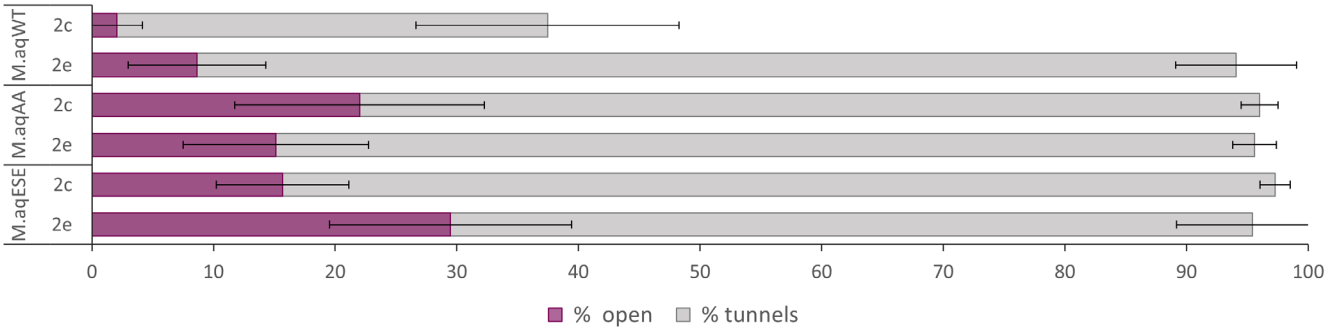

Figure S9: Availability and opening of the substrate tunnels 2c and 2e (in %) in M.aqWT and the variants M.aqAA and M.aqESE. The tunnel availability was defined as the rate of snapshots, over the entire MDs, where the respective tunnels were detected (for a minimum radius ≥ 0.9 Å), while the tunnel opening was defined as the rate of snapshots presenting the respective tunnels with minimum radii ≥ 1.4 Å.

Table S3. Parameters of the tunnels and B-factors of the relevant loops averaged over five individual MD simulations of M.aqWT and M.aqESE and three individual simulations for the variant M.aqAA.

	M.aqWT		M.aqAA		M.aqESE	
Mutations[a]	-		V141A, M228A		Q129E, V141S, M228E	
Tunnel	**2c**	**2e**	**2c**	**2e**	**2c**	**2e**
Tunnels [%]	37.5 ± 10.8	94.1 ± 5.0	96.0 ± 1.5	95.6 ± 1.8	97.3 ± 1.3	95.4 ± 6.2
Tunnels open [%]	2.1 ± 2.1	8.6 ± 5.6	22.0 ± 10.2	15.1 ± 7.6	15.7 ± 5.4	29.5 ± 10.0
Bottleneck radius [Å]	1.09 ± 0.15	1.19 ± 0.14	1.27 ± 0.15	1.23 ± 0.15	1.22 ± 0.16	1.26 ± 0.16
Length [Å]	26.5 ± 3.7	19.3 ± 1.9	24.0 ± 2.4	19.5 ± 2.0	25.2 ± 2.7	18.9 ± 2.1
Loop	**BC**	**FG**	**BC**	**FG**	**BC**	**FG**
B-factor peak	109.9 ± 44.4	30.4 ± 2.9	65.6 ± 3.4	61.4 ± 35.3	106.2 ± 99.9	28.1 ± 17.3

[a]The mutations introduced in the enzyme with respect to the wild type M.aqWT; data was collected as averages from 100 000 frames (60 000 for M.aqAA) for the tunnels found using a probe of 0.9 Å radius, presented with the respective standard deviations. Tunnels were defined as open with a bottleneck threshold ≥ 1.4 Å radius. Tunnel nomenclature was applied from Cojocaru *et al*.[22]

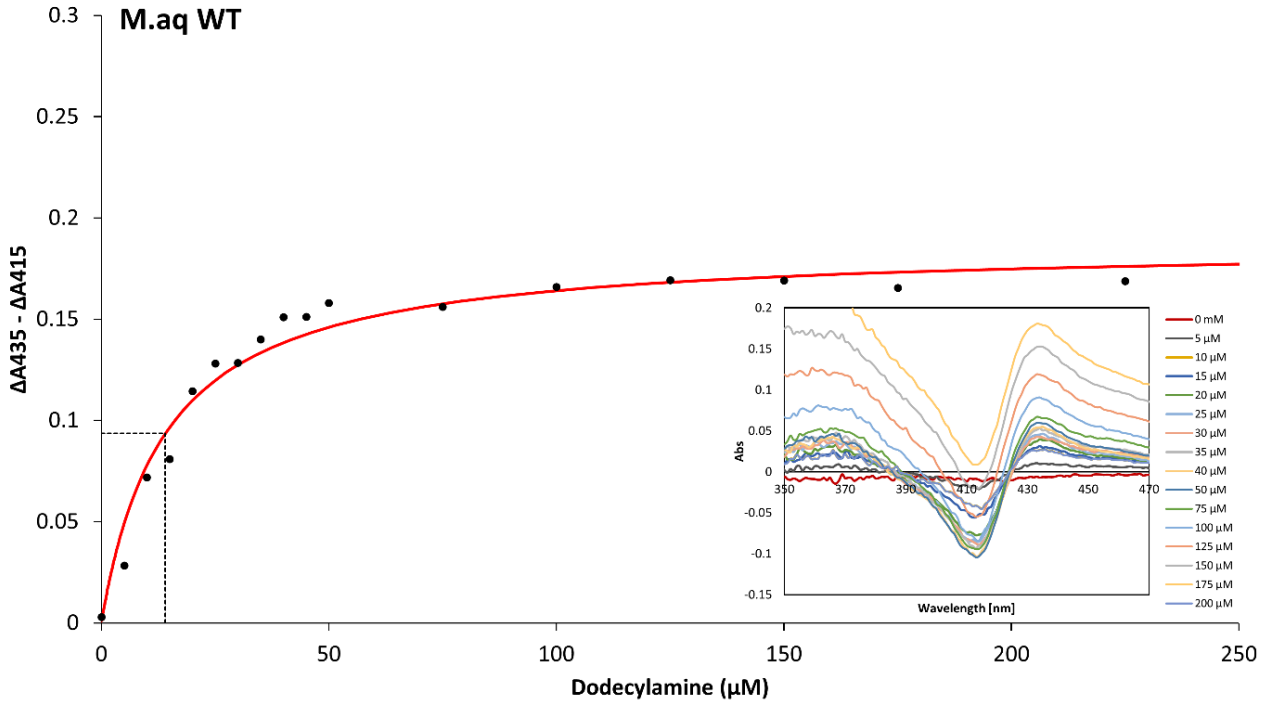

Figure S10: Spin state difference spectra of M.aqWT using dodecylamine as ligand. Varying concentrations were added to a 1 µM P450 solution until substrate saturation (A_{max}) was reached. The spin shift ΔA was calculated by subtraction of the reference sample (P450 without dodecylamine).

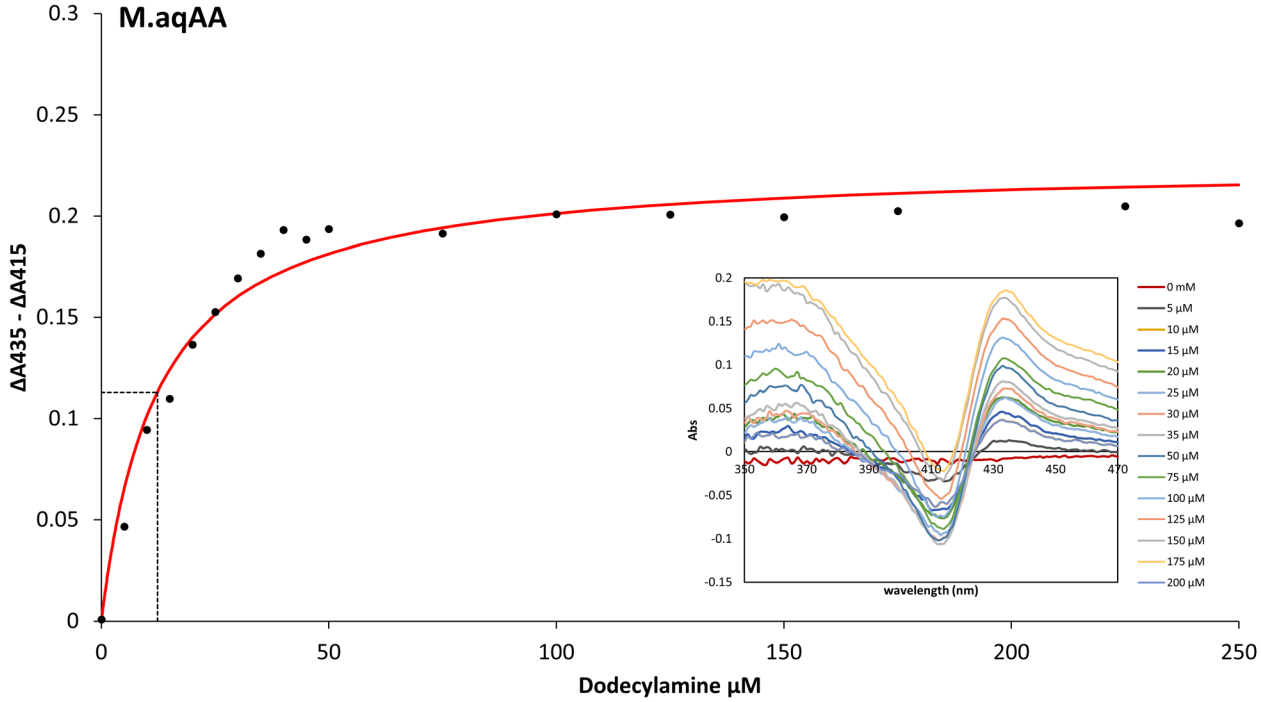

Figure S11: Spin state difference spectra of M.aqAA using dodecylamine as ligand. Varying concentrations were added to a 1 µM P450 solution until substrate saturation (A_{max}) was reached. The spin shift ΔA was calculated by subtraction of the reference sample (P450 without dodecylamine).

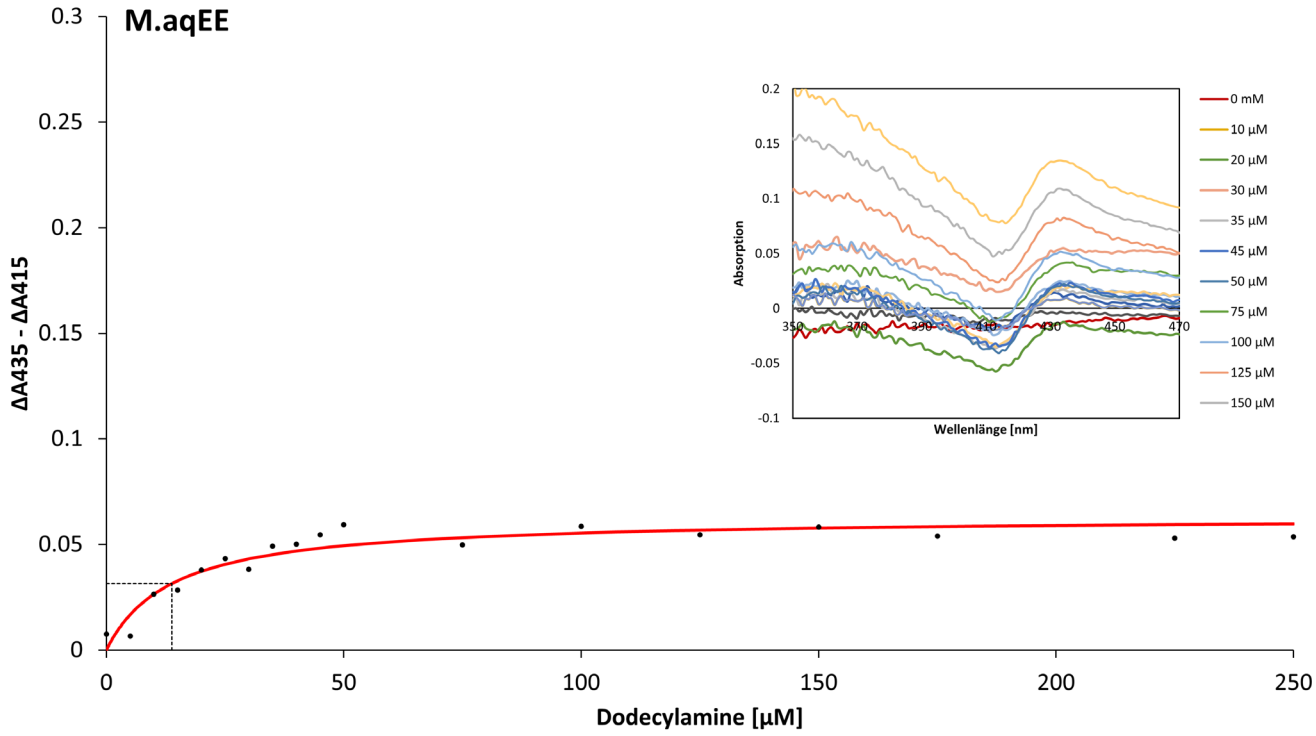

Figure S12: Spin state difference spectra of M.aqEE using dodecylamine as ligand. Varying concentrations were added to a 1 µM P450 solution until substrate saturation (A_{max}) was reached. The spin shift ΔA was calculated by subtraction of the reference sample (P450 without dodecylamine).

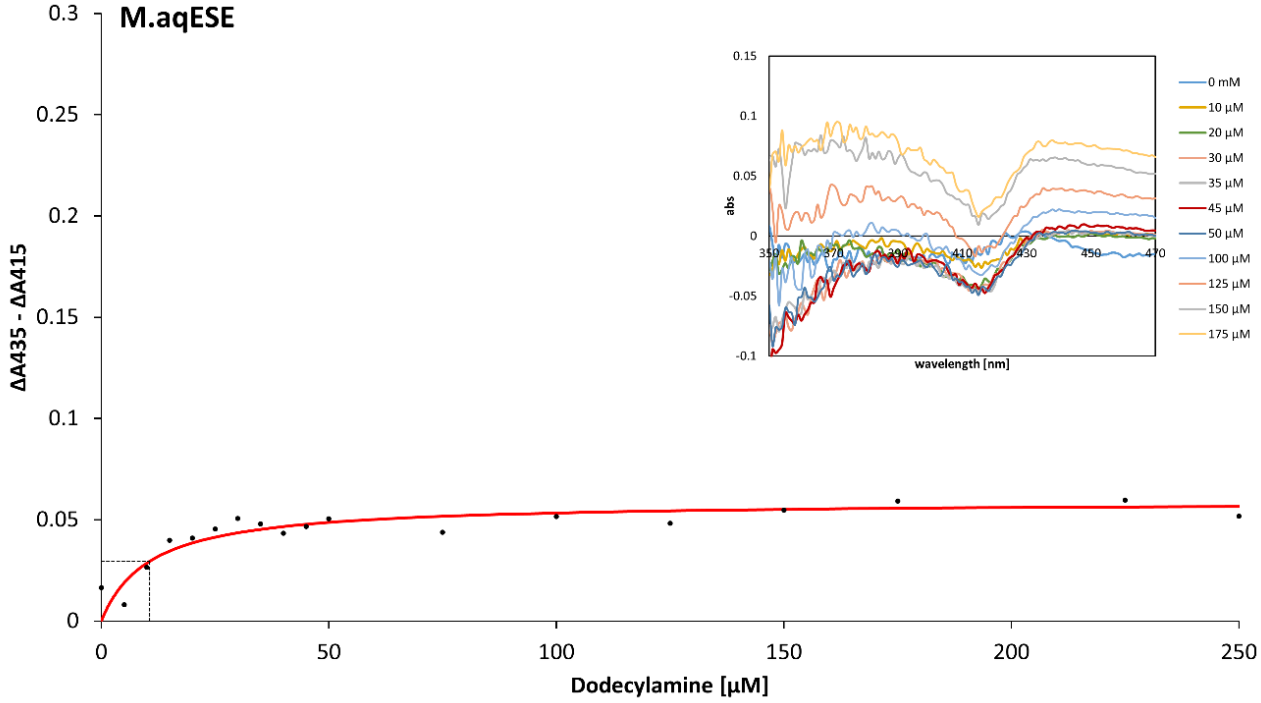

Figure S13: Spin state difference spectra of M.aqESE using dodecylamine as ligand. Varying concentrations were added to a 1 µM P450 solution until substrate saturation (A_{max}) was reached. The spin shift ΔA was calculated by subtraction of the reference sample (P450 without dodecylamine).

Table S4: Dissociation constants and absorbance maxima of the respective enzymes.

	M.aqWT	M.aqAA	M.aqEE	M.aqESE
A_{max}	0.19	0.23	0.06	0.06
K_d	14.10	12.32	13.80	10.60

For determination of the dissociation constant K_d, ΔA was plotted against the applied substrate concentration and fitted in Excel using a hyperbolic curve as described by Klenk *et al*.[6] The measurements were performed in triplicates and averaged.

References

(1) Hoffmann, S. M.; Weissenborn, M. J.; Gricman, Ł.; Notonier, S.; Pleiss, J.; Hauer, B. The Impact of Linker Length on P450 Fusion Constructs: Activity, Stability and Coupling. *ChemCatChem* **2016**, *8* (8), 1591–1597. https://doi.org/10.1002/cctc.201501397.

(2) Hoffmann, S. M. Studien Zur Optimierung Der Katalyse Mittels Der Monooxygenase CYP153A M.Aq, 2017. https://doi.org/http://dx.doi.org/10.18419/opus-9932.

(3) Kille, S.; Acevedo-Rocha, C. G.; Parra, L. P.; Zhang, Z. G.; Opperman, D. J.; Reetz, M. T.; Acevedo, J. P. Reducing Codon Redundancy and Screening Effort of Combinatorial Protein Libraries Created by Saturation Mutagenesis. *ACS Synth. Biol.* **2013**, *2* (2), 83–92. https://doi.org/10.1021/sb300037w.

(4) OMURA, T.; SATO, R. THE CARBON MONOXIDE-BINDING PIGMENT OF LIVER MICROSOMES. I. EVIDENCE FOR ITS HEMOPROTEIN NATURE. *J. Biol. Chem.* **1964**, *239* (7), 2370–2378.

(5) R. Rapp, L.; M. Marques, S.; Zukic, E.; Rowlinson, B.; Sharma, M.; Grogan, G.; Damborsky, J.; Hauer, B. Substrate Anchoring and Flexibility Reduction in CYP153AM.Aq Leads to Highly Improved Efficiency toward Octanoic Acid. *ACS Catal.* **2021**, *11* (5), 3182–3189. https://doi.org/10.1021/acscatal.0c05193.

(6) Klenk, J. M.; Ertl, J.; Rapp, L.; Fischer, M. P.; Hauer, B. Expression and Characterization of the Benzoic Acid Hydroxylase CYP199A25 from Arthrobacter Sp. *Mol. Catal.* **2020**, *484*. https://doi.org/10.1016/j.mcat.2019.110739.

(7) Hanwell, M. D.; Curtis, D. E.; Lonie, D. C.; Vandermeerschd, T.; Zurek, E.; Hutchison, G. R. Avogadro: An Advanced Semantic Chemical Editor, Visualization, and Analysis Platform. *J. Cheminform.* **2012**, *4* (17). https://doi.org/10.1186/1758-2946-4-17.

(8) Sanner, M. F. Python: A Programming Language for Software Integration and Development. *J. Mol. Graph. Model.* **1999**, *17* (1), 57–61.

(9) Shahrokh, K.; Orendt, A.; Yost, G. S.; Cheatham, T. E. Quantum Mechanically Derived AMBER-Compatible Heme Parameters for Various States of the Cytochrome P450 Catalytic Cycle. *J. Comput. Chem.* **2012**, *33* (2), 119–133. https://doi.org/10.1002/jcc.21922.

(10) Trott, O.; Olson, A. J. AutoDock Vina: Improving the Speed and Accuracy of Docking with a New Scoring Function, Efficient Optimization, and Multithreading. *J. Comput. Chem.* **2009**, *31* (2), 455–461. https://doi.org/10.1002/jcc.21334.

(11) Case, D. A.; Babin, V.; Berryman, J. T.; Betz, R. M.; Cai, Q.; Cerutti, D. S.; Cheatham III, T. E.; Darden, T. A.; Duke, R. E.; Gohlke, H.; Goetz, A. W.; Gusarov, S.; Homeyer, N.; Janowski, P.; Kaus, J.; Kolossváry, I.; Kovalenko, A.; Lee, T. S.; LeGrand, S.; Luchko, T.; Luo, R.; Madej, B.; Merz, K. M.; Paesani, F.; Roe, D. R.; Roitberg, A.; Sagui, C.; Salomen-Ferrer, R.; Seabra, G.; Simmerling, G. L.; Smith, W.; Swails, J.; Walker, R. C.; Wang, J.; Wolf, R. M.; Wu, X.; Kollman, P. A. AMBER14. *AMBER 14*. 2014.

(12) Nguyen, H.; Maier, J.; Huang, H.; Perrone, V.; Simmerling, C. Folding Simulations for Proteins with Diverse Topologies Are Accessible in Days with a Physics-Based Force Field and Implicit Solvent. *J. Am. Chem. Soc.*

2014, *136* (40), 13959–13962. https://doi.org/10.1021/ja5032776.

(13) Izadi, S.; Onufriev, A. V. Accuracy Limit of Rigid 3-Point Water Models. *J. Chem. Phys.* **2016**, *145* (7). https://doi.org/10.1063/1.4960175.

(14) Götz, A. W.; Williamson, M. J.; Xu, D.; Poole, D.; Le Grand, S.; Walker, R. C. Routine Microsecond Molecular Dynamics Simulations with AMBER on GPUs. 1. Generalized Born. *J. Chem. Theory Comput.* **2012**, *8* (5), 1542–1555. https://doi.org/10.1021/ct200909j.

(15) Le Grand, S.; Götz, A. W.; Walker, R. C. SPFP: Speed without Compromise - A Mixed Precision Model for GPU Accelerated Molecular Dynamics Simulations. *Comput. Phys. Commun.* **2013**, *184* (2), 374–380. https://doi.org/10.1016/j.cpc.2012.09.022.

(16) Andricioaei, I.; Karplus, M. Particle Mesh Ewald: An N·log(N) Method for Ewald Sums in Large Systems The. *Stat. Mech. Fluid Mix. J. Chem. Phys.* **1993**, *98* (12). https://doi.org/10.1063/1.1401821.

(17) Ryckaert, J. P.; Ciccotti, G.; Berendsen, H. J. C. Numerical Integration of the Cartesian Equations of Motion of a System with Constraints: Molecular Dynamics of n-Alkanes. *J. Comput. Phys.* **1977**, *23* (3), 327–341. https://doi.org/10.1016/0021-9991(77)90098-5.

(18) Roe, D. R.; Cheatham, T. E. PTRAJ and CPPTRAJ: Software for Processing and Analysis of Molecular Dynamics Trajectory Data. *J. Chem. Theory Comput.* **2013**, *9* (7), 3084–3095. https://doi.org/10.1021/ct400341p.

(19) DeLano, W. L. The PyMOL Molecular Graphics System, Version 1.8. *Schrödinger LLC* **2014**, http://www.pymol.org. https://doi.org/10.1038/hr.2014.17.

(20) Humphrey, W.; Dalke, A.; Schulten, K. VMD: Visual Molecular Dynamics. *J. Mol. Graph.* **1996**, *14* (1), 33–38. https://doi.org/10.1016/0263-7855(96)00018-5.

(21) Chovancova, E.; Pavelka, A.; Benes, P.; Strnad, O.; Brezovsky, J.; Kozlikova, B.; Gora, A.; Sustr, V.; Klvana, M.; Medek, P.; Biedermannova, L.; Sochor, J.; Damborsky, J. CAVER 3.0: A Tool for the Analysis of Transport Pathways in Dynamic Protein Structures. *PLoS Comput. Biol.* **2012**, *8* (10). https://doi.org/10.1371/journal.pcbi.1002708.

(22) Cojocaru, V.; Winn, P. J.; Wade, R. C. The Ins and Outs of Cytochrome P450s. *Biochim. Biophys. Acta - Gen. Subj.* **2007**, *1770* (3), 390–401. https://doi.org/10.1016/j.bbagen.2006.07.005.